Initial Development of Thermal and Stress Fields in Continuously Cast Steel Billets

J. E. KELLY, K. P. MICHALEK, T. G. O'CONNOR, B. G. THOMAS, and J. A. DANTZIG

A mathematical model has been developed to compute the thermomechanical state of the shell of continuously cast steels in a round billet casting mold. The model determines the temperature distributions, the stresses in and the gap between the casting mold and the solidifying strand. The effect of variations in steel carbon content and mold taper on the thermal, displacement, and stress fields are examined. Comparisons with available experimental observations verify the predictions of the model. The model demonstrates that the thermal shrinkage associated with the phase change from delta-ferrite to austenite in 0.1 pct C steel accounts for the decreased heat transfer observed in that alloy, as well as its susceptibility to cracking.

I. INTRODUCTION

CONTINUOUS casting now accounts for over 50 pct of domestic steel production in the United States and over 90 pct of the steel production in Japan. The conversion to continuous casting from ingot casting has been driven by the improved yield, thermal efficiency, and higher quality available in the newer process. To help achieve these gains, the process has been mathematically modeled to increase the understanding of the roles of important variables in the process, improve design of continuous casting machines, and eliminate casting defects.

The defects to which continuously cast billets are susceptible include longitudinal and transverse surface cracks and subsurface cracks. Although the specifics depend on both the defect and the casting system, their primary cause is the interaction between heat transfer in the mold and the solidification and concomitant shrinkage of the billet.

Over the years, many mathematical models have been developed to help determine the origin of, and assess means for controlling, these defects. The aspect of the problem which makes building a mathematical model for the heat transfer difficult is that the effective heat transfer between the billet and the mold is largely determined by the size of the air gap between them, caused by the thermal distortion of both the billet and the mold. Because the size of the gap depends on the respective temperature distributions, the formulations for the problems of air gap formation and temperature are coupled.

To overcome this problem, a number of researchers have estimated values for the heat transfer coefficients. It is common practice to divide the billet into two or more heat transfer zones. The upper zone has a high heat transfer coefficient to characterize the good thermal contact between the billet and the mold, perhaps mediated by a mold lubricant or flux. The lower region of the mold is characterized by smaller heat transfer coefficients, associated with the air gap. The magnitude and locations of these regions vary from author to author,[1,2] based on experimental observations and/or educated guesses.

A second popular means for determining the heat transfer characteristics is to analyze experimental data gathered in plant trials.[3,4] Typically, thermocouples or pairs of thermocouples are placed in the mold at various locations and their response is used to determine the temperature distribution in the mold and, in particular, to compute the heat flux on the inside face of the mold. These heat fluxes are then incorporated as boundary conditions for the heat flow problem in the continuously cast strand.

The difficulty in applying either of the above methods arises when one wishes to use the mathematical model to assess the importance of changes in the process variables on the solidification characteristics of the billet. It is not easy to alter the estimated heat transfer coefficients and be confident that the new estimates truly represent what would happen in the new configuration. Similarly, the heat fluxes measured under one set of experimental conditions may not be appropriate for the new set of experimental conditions, but it is difficult to tell *a priori* how large or how small the error introduced by using them will be.

In a few analyses[5,6] the air gap was calculated by combining thermal and stress analysis, following the progress of a two-dimensional slice of the strand down through the mold. Grill *et al.*[5] used experimental data to estimate the heat flow at the mid-face of a slab, and calculated gap formation at its corners. Kristiansson[6] simulated a billet casting, using stress analysis to determine the size of the shell/mold gap over the entire periphery of the strand. In the latter analysis, the gap computed by the stress program at the previous step was used as a boundary condition for the next step of the heat flow model. Although this approach represents a marked improvement over previous models, neither analysis considered explicitly the heat flow or displacement of the casting mold, which has been shown by Samarasekera *et al.*[4] to have a significant effect on the solution.

In the present work, an attempt is made to improve this situation by developing models to compute temperature distributions in both the billet and the mold. These models also directly compute the air gap, *via* stress analysis, to obtain a self-consistent solution. The analysis has been restricted thus far to round castings to maintain the economy of a two-

J. E. KELLY and T. G. O'CONNOR, Graduate Students, and B. G. THOMAS, Assistant Professor, and J. A. DANTZIG, Associate Professor, are with the Department of Mechanical and Industrial Engineering, University of Illinois at Urbana-Champaign, 1206 West Green Street, Urbana, IL 61801. K. P. MICHALEK, formerly Graduate Student, Department of Mechanical and Industrial Engineering, University of Illinois at Urbana-Champaign, is with AT&T, Room 20505, 200 Laurel Avenue, Middletown, NJ 07748.

Manuscript submitted March 11, 1987.

dimensional axisymmetric formulation, and by the assumption of steady state, again to reduce computation. This last restriction obviates the study of some important phenomena, such as meniscus and oscillation mark formation. Nevertheless, many of the remaining aspects of continuous casting can and have been retained. The procedures for the analysis are described in the next section.

II. MODEL DESCRIPTION

A. *Overview*

The model for heat transfer between the mold and strand is characterized by heat transfer coefficients across the air gap. These heat transfer coefficients, described in detail in a later section, include heat transferred by both conduction and radiation, as they depend upon the temperatures of both the ingot and the mold, the size of the air gap, the conductivity of the gases in the gap, and an assumed contact resistance when the steel and mold touch near the meniscus. The change from direct contact to the development of a gap is determined in the analysis by calculating the temperature, displacement, and stress fields in the billet and the mold.

The following strategy was used to obtain the solution:

BEGIN

(a) build a finite element model of the casting and mold;
(b) compute a velocity field in the billet;
(c) define a starting set of heat transfer coefficients;

ELASTIC CYCLE

(d) compute temperatures in both the mold and the strand from the velocity solution and heat transfer coefficients;
(e) compute elastic stress solutions for the mold and solid portion of the strand from the thermal solution;
(f) recompute heat transfer coefficients from the gaps computed in stress solution;
(g) cycle through steps (d) through (f) until a self-consistent solution is found;

ELASTIC-PLASTIC CYCLE

(h) compute an elastic-plastic stress solution beginning with the latest converged temperature/stress solution;
(i) recompute the heat transfer coefficients from the elastic-plastic solution;
(j) compute a new thermal solution; and
(k) cycle through steps (h) through (j) until the final self-consistent solution is obtained.

Each of the steps in the above strategy is discussed in more detail below. Since the analysis to date has been done only for axisymmetric billets, the model description is given in that context.

The finite element method (FEM) was chosen for this analysis owing to the availability of commercial computer codes for the velocity, thermal and stress analyses. The problem geometry and boundary conditions are shown in Figures 1(a) and (b). The velocity and thermal analyses were carried out with FIDAP,[7] and the stress analysis was done with NIKE2D[8] modified to run on a UNIX-based system. The FEM mesh was built using FIMESH, the mesh generator in FIDAP, with four-noded linear isoparametric quadrilateral elements.

A series of translator programs were written to pass the mesh and thermal solution to NIKE2D for stress analysis and to recompute heat transfer coefficients from the stress solution and pass them back to FIDAP. Details of the velocity, thermal and stress solutions are given below. In all cases, the physical properties of the materials—specific heat, thermal conductivity, elastic modulus, strain dependent flow stress, and thermal expansion coefficient—were temperature dependent, and the values used are tabulated in Appendix B. The latent heat of fusion was distributed over the freezing range as an additional specific heat.

B. *Velocity Solution*

The velocities were obtained by solving the problem posed in Figure 1(a). On the upper surface of the billet, the downward inlet velocity was specified as a parabolic function over the narrow region corresponding to the downspout, and the normal velocity was set to zero on the remainder of the free surface. The radial velocity was set to zero on the centerline. On the vertical surface of the billet, the axial velocity was set to the casting speed. The outlet velocity was unspecified, which corresponds to a shear stress-free boundary in the FEM, and allows mass to be conserved in the strand.

The velocity distribution was computed using FIDAP, ignoring all of the inertial terms in the momentum transport equations. Although it is well known that these inertial terms are important, and that the flow in the liquid portion of the billet is turbulent, it has also been repeatedly shown that in most cases the details of the flow field in the liquid are not important to the overall heat transfer and that the enhanced thermal dissipation due to convection can be adequately accounted for by an increased thermal conductivity.[9] Any hope of examining shell erosion by the incoming stream is lost, of course.

C. *Thermal Solution*

The FEM form of the energy equation after the transient terms have been removed is given by

$$([A(U)] + [K(T)])\{T\} = \{F(T)\} \qquad [1]$$

where $[A(U)]$ represents the contributions to the global conductance matrix from advection of energy (convective transport)
$[K(T)]$ represents the contributions to the global conductance matrix from diffusion of energy (conduction)
$\{F(T)\}$ represents the forcing function for energy (heat fluxes, convection to the environment, *etc.*)
$\{T\}$ is the vector of nodal temperatures

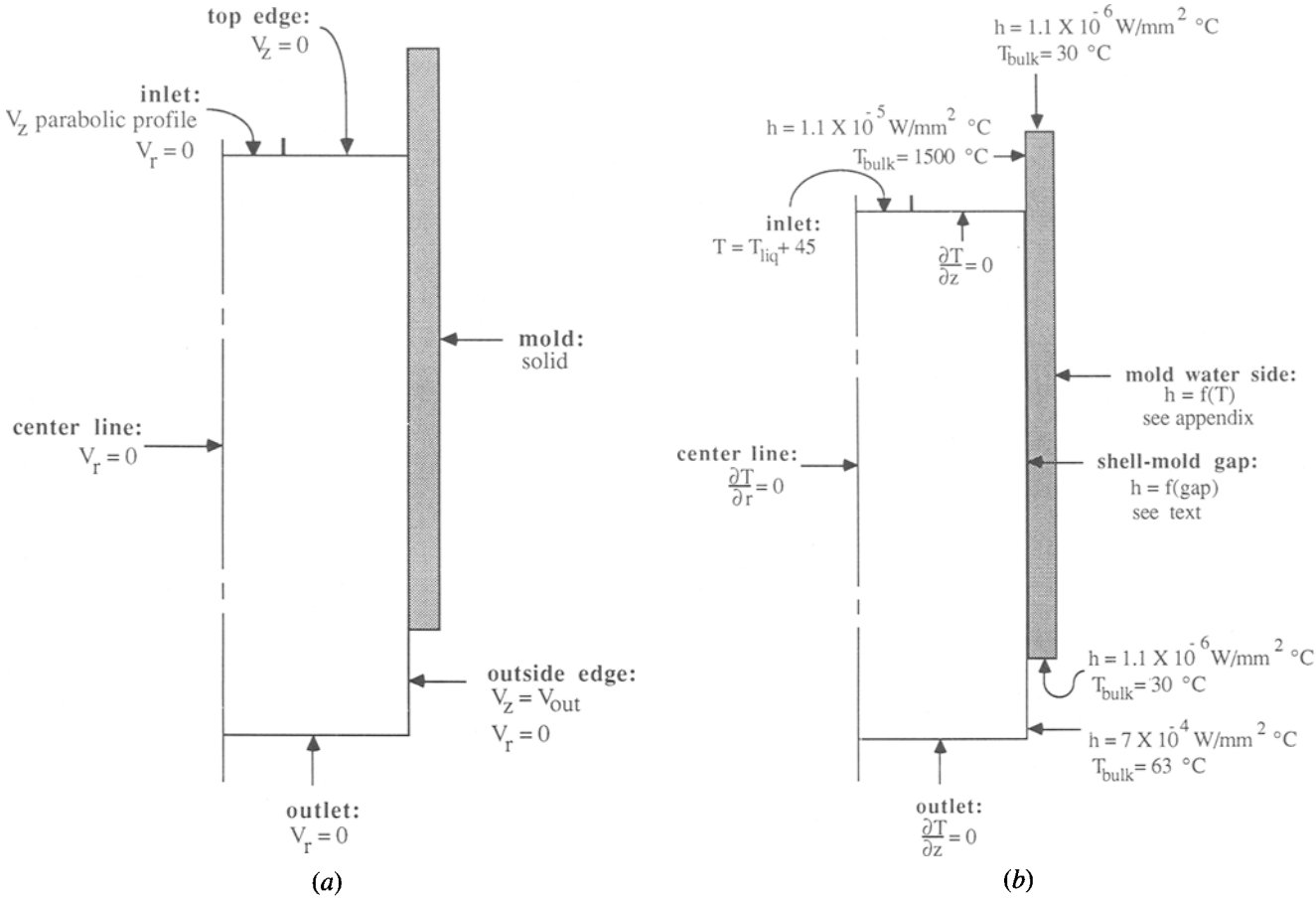

Fig. 1—(*a*) Boundary conditions for the velocity problem. (*b*) Boundary conditions for the temperature problem.

The FEM formulations for $[A]$, $[K]$, and $\{F\}$ can be found in Reference 7. The dependence of $[K]$ and $\{F\}$ on temperature makes the problem nonlinear, so that an iterative solution is required. It was found that the large discontinuity in specific heat associated with the latent heat of fusion could lead to convergence difficulties, requiring the use of carefully controlled solution procedures.

Two of the solution strategies available in FIDAP were used in sequence: successive substitution with relaxation, and a variant of Newton's method. After iteration i, Eq. [1] can be written as

$$([A(U)] + [K(T_i)])\{T^*\} = \{F(T_i)\} \qquad [2]$$

where T_i is the solution vector at iteration i, and $\{T^*\}$ is obtained by solving Eq. [2]. In the successive substitution method with relaxation, $\{T_{i+1}\}$ is given by

$$\{T_{i+1}\} = \alpha\{T_i\} + (1 - \alpha)\{T^*\} \qquad [3]$$

where α is an "acceleration" or "relaxation" factor. The convergence rate was found to be highly dependent on the choice of α, as shown in Figure 2.

In Newton's method, the residual error after iteration i is used to select the next estimate for $\{T_{i+1}\}$. After iteration i, the residual error $\{R_i\}$ is given by

$$\{R_i\} = ([A(U) + [K(T_i)])\{T_i\} - \{F(T_i)\} \qquad [4]$$

The estimate for $\{T_{i+1}\}$ is then

$$\{T_{i+1}\} = \alpha\{T_i\} + (1 - \alpha)(\{T_i\} - [\mathbf{J}(T_i)]^{-1}\{R_i\}) \qquad [5]$$

where $\mathbf{J} = \partial\{R\}/\partial\{T\}$ is the Jacobian for the system of equations. The details for this method, including efficient algorithms for computing the Jacobian, are described in Reference 7. Converged solutions were achieved in the present analysis by using successive substitution for the first five iterations, followed by a variation on the Newton method, called the "Quasi-Newton" method in FIDAP, for subsequent iterations, keeping $\alpha = 0.5$ throughout. As seen in Figure 2, this scheme provided the fastest convergence of all the methods compared in this study.

The first simulation was started with $\{T\} = 0$ everywhere, and 13 iterations were required to reach convergence. For this first run, all the heat transfer coefficients were chosen to be the value associated with direct contact, discussed in the next section. Subsequent simulations (using new heat transfer coefficients) were restarted from the earlier solution, and typically took six or seven iterations to converge. The solution was accepted when the relative errors in both the temperatures and the residuals were less than 10^{-4} (see Reference 7).

D. *Elastic Stress Analysis*

The temperatures calculated by FIDAP were then used as input to NIKE2D to perform separate elastic stress analyses

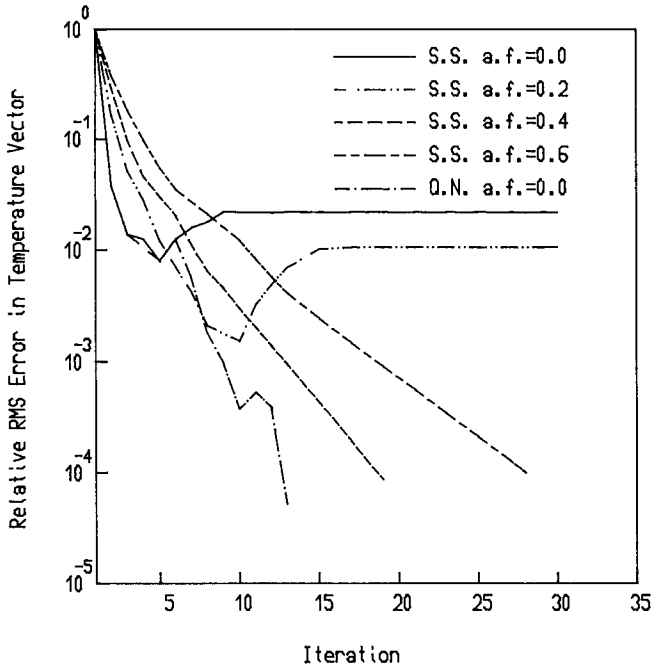

Fig. 2—Relative error in temperature *vs* iteration for various solution strategies. Solution was accepted when the relative error was less than 0.0001. (S.S. = successive substitution; Q.N. = Quasi-Newton; a.f. = acceleration factor)

on the mold and solid shell. The nonuniform temperature distribution causes both the mold and the shell to distort from their reference configurations, leading to the air gap. In the present analysis, thermal distortion of the casting mold was computed *via* elastic stress analysis, using the boundary conditions indicated in Figure 3(a). The mold tube was left essentially unconstrained along its length from the small strains produced by thermal expansion and contraction, corresponding to the constraint condition imposed on a mold clamped in place on the mold table.[10]

Figure 3(b) also indicates that the mesh within the strand was altered for the stress analysis by stripping away all of

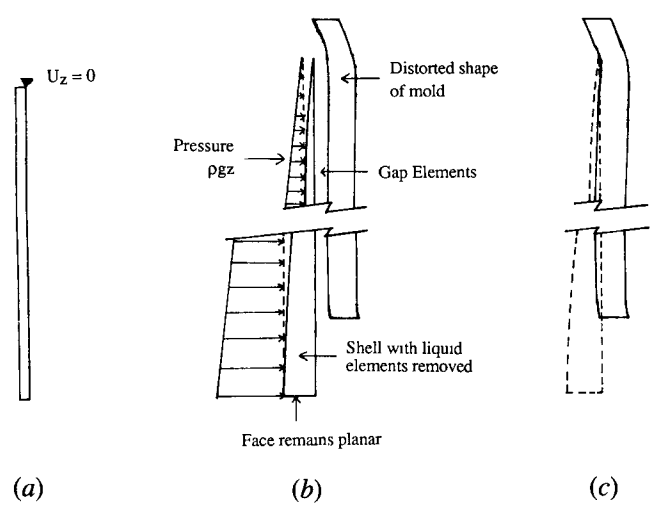

Fig. 3—(*a*) Upper corner of mold constrained, corresponding to clamping on mold table. (*b*) Juxtaposition of distorted mold and shell in its original location, showing ferrostatic head boundary condition. (*c*) Distorted mold and shell in its corrected reference configuration.

the elements which were entirely liquid, and replacing them with a pressure corresponding to the metallostatic head. Because liquid steel at the meniscus is always free to run out to the mold, the reference configuration for the strand must be based on the *distorted* shape of the mold. To achieve this, an elastic stress analysis was first performed for the mold, then all of the remaining nodes in the shell were moved outward by the calculated amount of distortion in the mold at the meniscus, to establish the initial state shown in Figure 3(c). The effect of this movement on the thermal solution is insignificant because the displacement is so small; but it is crucial to the stress solution, because it ensures that the first material to solidify will be stress free. The distorted shape of the shell was then computed, using temperature dependent elastic moduli, but neglecting plastic deformation.

E. *Adaptive Refinement of Heat Transfer Coefficients*

New estimates for the air gaps were obtained from the displacement solutions for the mold and shell. The local heat transfer coefficient, h, was assumed to be related to the gap by[5]

$$h = K_g/gap + h_{\text{rad}} \qquad [6]$$

where K_g is the thermal conductivity of the gap medium, gap is the thickness of the gap, and h_{rad} is the contribution from radiation. This equation was developed specifically to simulate volatile lubricants such as rapeseed oil. Details regarding the evaluation of K_g are given in Appendix A. The radiation term was computed assuming emissivities of 0.8 for both surfaces and accounts for less than 5 pct of the total h. If the value of h computed from Eq. [6] exceeded the value associated with direct contact, it was replaced by that value. The h for direct contact was taken to be 6×10^{-3} W/(mm^2 K). Discussion of the determination of this value is given in the Results section. This corresponds to a gap of approximately 0.0125 mm, depending on the gap temperatures.

The new heat transfer coefficients were then reinserted into the thermal analysis, and "cycles" of heat transfer/stress analysis were repeated until the gaps stopped changing within the following tolerance:

$$\frac{\sqrt{\sum_{\text{all gaps}} (gap_{\text{old}} - gap_{\text{new}})^2}}{\sqrt{\sum_{\text{all gaps}} gap_{\text{new}}^2}} < 0.01 \qquad [7]$$

If the most recently computed gaps were entered directly in Eq. [6], it was found that the succession of computed gaps did not converge. Accordingly, the most recently computed gaps were "relaxed" to obtain more stable estimates of the gaps for the next iteration, *viz.*,

$$gap_{\text{est}} = \alpha_g gap_{\text{last}} + (1 - \alpha_g) gap_{\text{new}} \qquad [8]$$

where α_g was 0.8 for most analyses. Using this method, a fully converged solution was typically achieved after 8 cycles.

F. *Elastic-Plastic Stress Analysis*

After convergence was achieved using elastic stress analyses for the shell, the procedure described above was redone,

treating the shell as an elastic-plastic material. This phase of the analysis typically required four additional cycles, using the same convergence criterion (Eq. [7]). Since the computed stresses in the mold were less than the yield point everywhere, except within a 2-mm radius semi-circle of the meniscus, the elastic solution was considered to be acceptable for the mold. It was found that the gap was relatively insensitive to the stress state in the billet, because the displacements are largely driven by thermal strains. Thus, the elastic solution was a good starting point for the elastic-plastic analysis of the shell.

In addition to the final temperatures themselves, the prior history of thermal loading is known to have an important influence on the resultant stress state.[11] The thermal load history of the strand was obtained by tracking the temperature of each node as it moved down the casting. The thermal load associated with the temperature change relative to the reference temperature (defined to be the solidus) was applied incrementally over 32 load steps. At each load step, an iterative solution was performed using the incremental strain method and a Quasi-Newton updating procedure,[8] typically taking four to seven iterations at each load step. Example thermal load histories at several locations in the strand are shown in Figure 4.

The mechanical properties used in the model, tabulated in Appendix B, were obtained from Wray.[12] The yield stress and elastic modulus were calculated from the flow stress data using an assumed yield strain of 0.1 pct. Flow stress data were chosen at a strain rate of $4 \times 10^{-4}\ s^{-1}$. This value was estimated *a posteori* from the computed strains, and is similar to the strain rates used by other researchers.[13]

Experimental data above 1200 °C were not available, leading us to use the following estimates. From 1200 °C to 40 °C below the solidus, the exponential extrapolation for flow stress at different strains suggested by Wray[12] was used to define plastic strain as a function of flow stress, temperature, and strain. From 40 °C below the solidus to the liquidus, the exponential extrapolation was reduced in 2 linear stages by multiplying by a factor which varied from 1 at 40 °C below the solidus to 0.1 at the solidus and to 0.01 at the liquidus. This temperature range corresponds to a region of greatly reduced ductility, with rupture strains between 0.1 pct and 0.3 pct.[13]

This procedure is somewhat arbitrary but it was found to remove effectively the load bearing ability of the steel in the mushy zone without unduly affecting convergence of the elastic-plastic solutions. The bilinear flow stress *vs* total strain curves that were generated as a function of temperature using the above procedure were input to the stress model (NIKE2D). The data are illustrated in Figure 5 for 0.7 pct carbon steel.

The thermal distortion of the billet and mold were calculated from the following equations:

$$\bar{\alpha}_{\text{thermal}} = \frac{\left(\frac{V}{V_{\text{ref}}}\right)^{1/3} - 1}{T - T_{\text{ref}}} \qquad [9]$$

$$\varepsilon_{\text{thermal}} = \bar{\alpha}_{\text{thermal}}(T - T_{\text{ref}}) \qquad [10]$$

where V_{ref} is the specific volume of the material at the reference temperature, T_{ref}, and V and T are the corresponding quantities at the present temperature. The specific volumes for the steels of interest (0.1 pct, 0.4 pct, and 0.7 pct C) were obtained from Wray,[14] as described in Appendix B. In each case, the reference temperature for the shell was chosen to be the solidus temperature for the alloy, and for the grades containing less than 0.17 pct C, there is a contribution from the volume change associated with the δ-γ phase transformation. The reference temperature for the copper mold was 25 °C.

Fracture criteria are not well defined for steel near the solidus. It is known that most steels exhibit very low ductility, fracturing at or soon after the yield point, near the solidus.[13,15] The extent of this low ductility range is very dependent on the grade of steel and the concentrations of trace elements such as phosphorus and sulfur, but in many cases it extends to about 70 °C below the solidus.

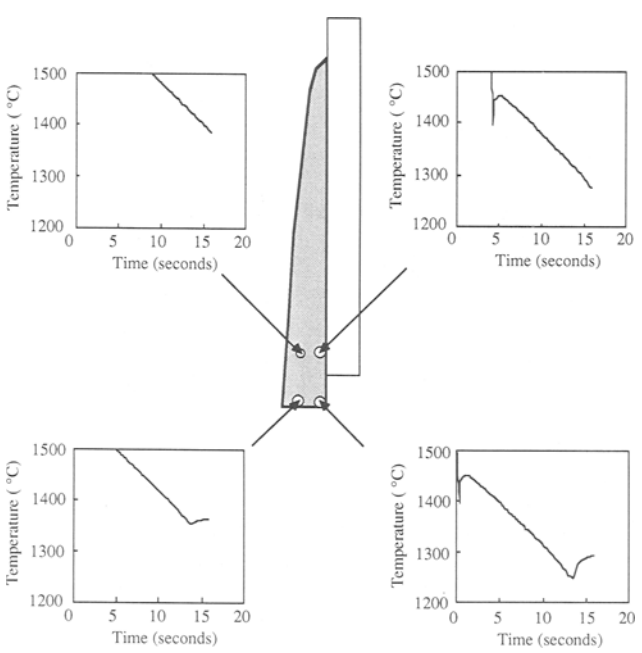

Fig. 4—Imposed thermal load histories at selected locations in the strand.

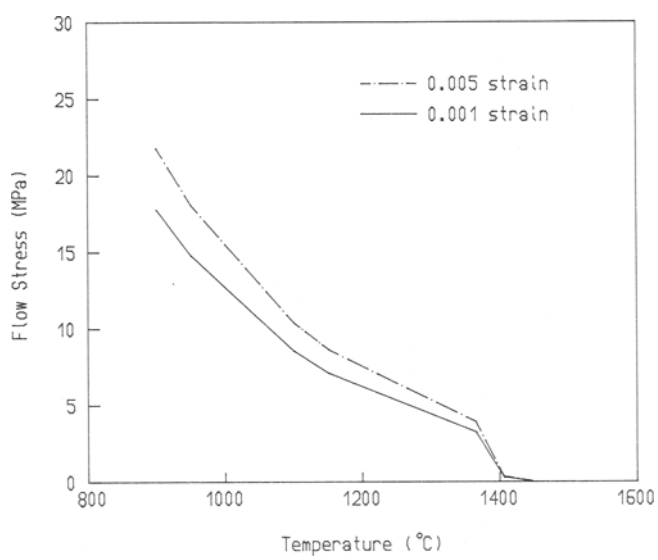

Fig. 5—Temperature *vs* flow stress at two strains for a strain rate of $0.0004\ s^{-1}$ for 0.7 pct plain carbon steel.[13]

Kristiansson,[6] and Sorimachi and Brimacombe[16] have used strain-based fracture criteria in this low ductility range, assuming that the material would fracture if the total mechanical strain exceeded 0.3 pct. In this analysis we chose simply to treat the steel near the solidus temperature as a brittle material, identifying crack susceptible locations as those where a tensile principal stress exceeded the yield stress and the temperature was within 70 °C of the solidus.

III. RESULTS

The model developed in the previous section was applied to simulate the continuous casting of steel in several different billet molds where previous experimental measurements were available. The first of these was a round billet mold, in which detailed temperature measurements had been made, as described in a series of recent papers[18,19,20] by researchers at Mannesmann AG. This casting mold, referred to hereafter as the Mannesmann mold, had an inside diameter of 182.8 mm at the top, tapering to 180.6 mm at the bottom of its 705 mm length (1.7 pct/m), and a wall thickness of 12 mm. Of the several grades of steel cast in the trials, the model was applied to the four cases of 0.1 pct C and 0.7 pct C cast at 25 mm/s and 50 mm/s. The FEM mesh, illustrated in Figure 6, contained 4526 nodes and 4360 elements in the billet, and 1560 nodes and 1575 elements in the mold.

Figure 7 illustrates the phenomena which occur in the first 10 mm of the mold. Note that the contact zone is extremely small, extending just a few millimeters below the meniscus. At high speed, there is a small extension of the liquidus onto the meniscus, suggesting that meniscus marks could form. At low speed, the calculations show that freezing over the meniscus is much more extensive, implying that much deeper meniscus marks are likely to form, as is often observed at lower speeds.

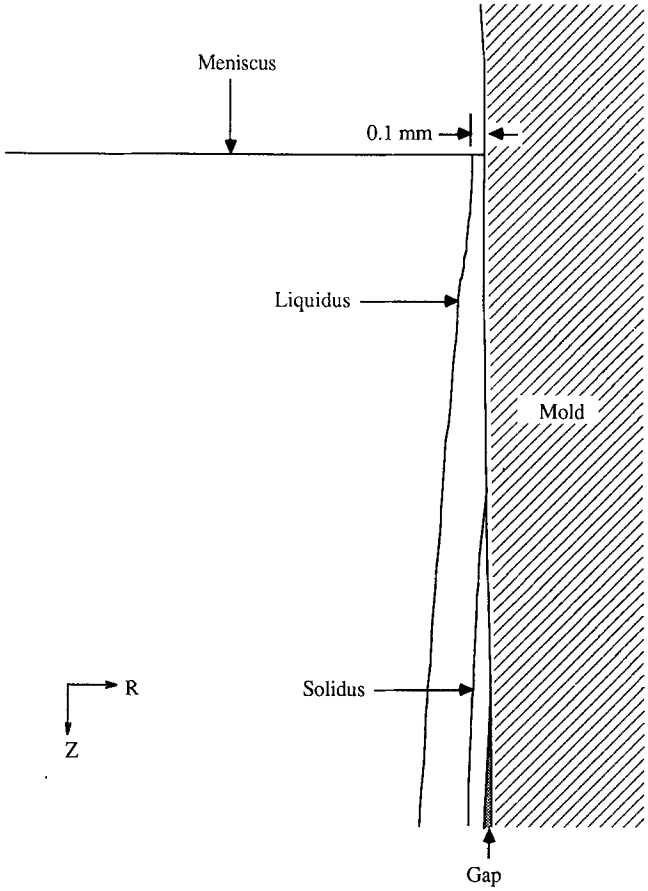

Fig. 7—Solidus and liquidus contours within 10 mm of the meniscus for 0.7 pct carbon steel. (Radial displacements of the mold and the shell have been multiplied by a factor of 10.)

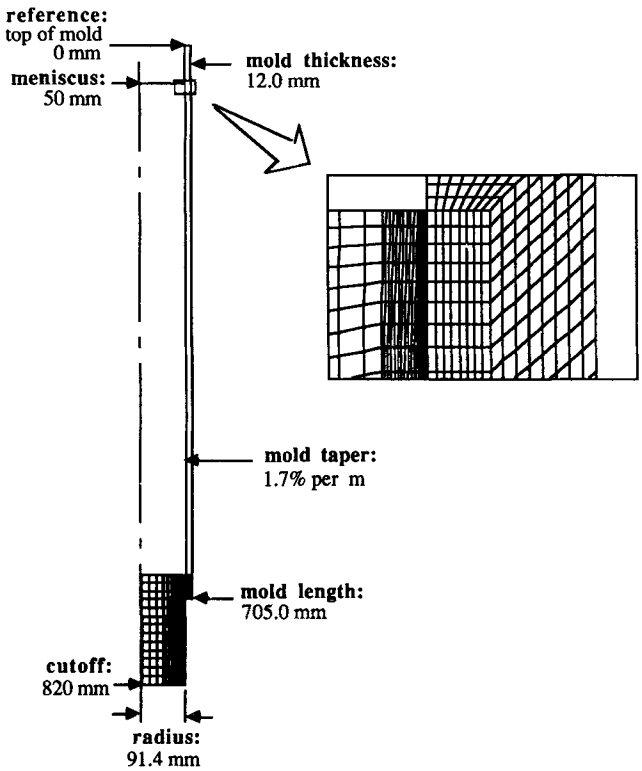

Fig. 6—Dimensions and selected portions of the finite element mesh for the Mannesmann mold.

Figure 8 shows comparisons of computed and measured temperatures at two depths into the mold wall along its length. The agreement between the computed and experimentally observed results is remarkably good. The magnitude and location of the peak temperatures, as well as the mild upward trend of temperatures toward the mold exit are all well predicted. The increase in mold wall temperature at the exit is due to the mold taper, as can be seen from the computed gap profile given in Figure 9. Separate calculations were performed assuming both $h = 0.003$ W/(mm^2 K) and $h = 0.006$ W/(mm^2 K) in the contact region. These values were chosen to cover the range of contact heat transfer coefficients that have been reported in the literature, all ranging between about 0.0025[6,21] to 0.006W/(mm^2 K).[22] There was little difference in the computed temperature profiles for 0.1 pct C steel. However, when $h = 0.003$W/(mm^2 K) for 0.7 pct C steel, the reduced heat fluxes from the billet led to the prediction that the shell would sieze against the mold wall at the mold exit, contrary to experimental observation, while simulations using the higher value did not predict recontact. Hence, $h = 0.006$ W/(mm^2 K) was adopted for the rest of the calculations described in this paper. Figure 10 shows the computed average heat fluxes at different casting speeds compared to measured values reported by Dubendorf *et al.*[18] The computed values agree very well for 0.7 pct C

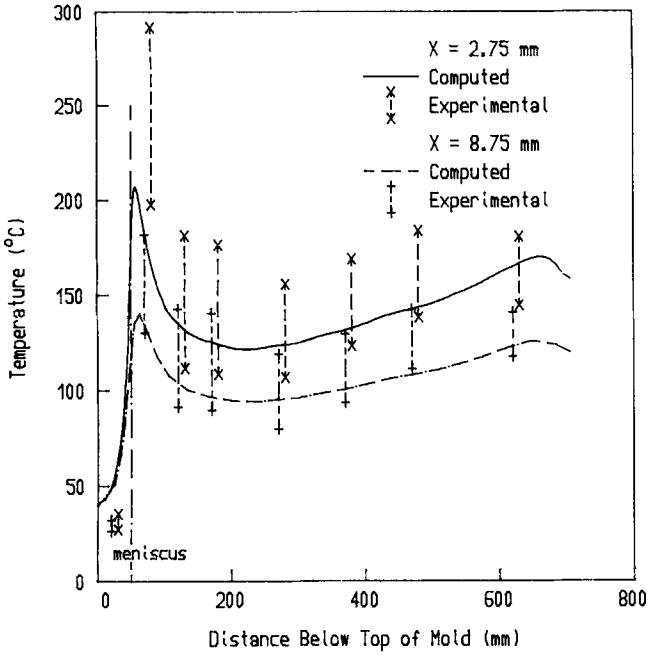

Fig. 8—Computed and experimentally measured temperature profiles at 2.75 mm and at 8.75 mm from the hot face of the Mannesmann mold. The maximum and minimum measured values at each location are shown.

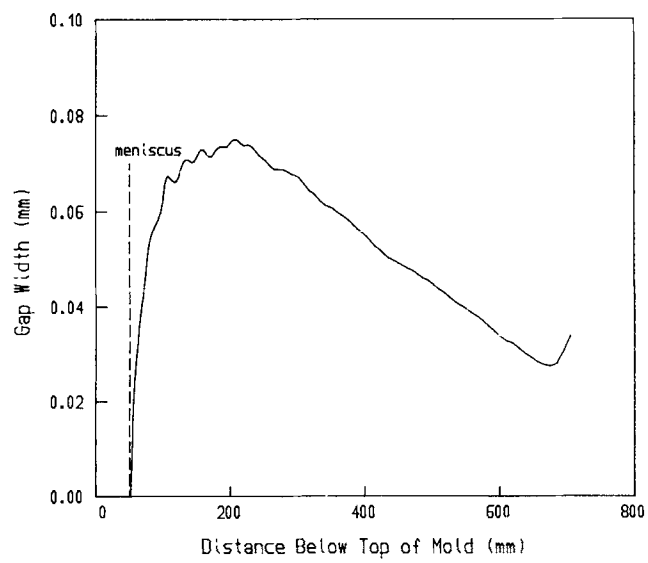

Fig. 9—The computed gap width profile for 0.1 pct C steel cast in the Mannesmann mold.

steel and are about 10 pct too low for 0.1 pct C steel. The trends are quite similar, however.

The model was next applied to examine several cases in the literature where thermal data had been obtained during casting of square billets. Thus, a measure of the applicability of axisymmetric models to other geometries could be obtained. Two mold geometries were examined. The first was based on a square billet mold described by Brimacombe *et al.*,[10] designated mold H142 in their paper. The axisymmetric idealization of this mold had an inside diameter of 111 mm, wall thickness of 9.53 mm, and length of 736 mm

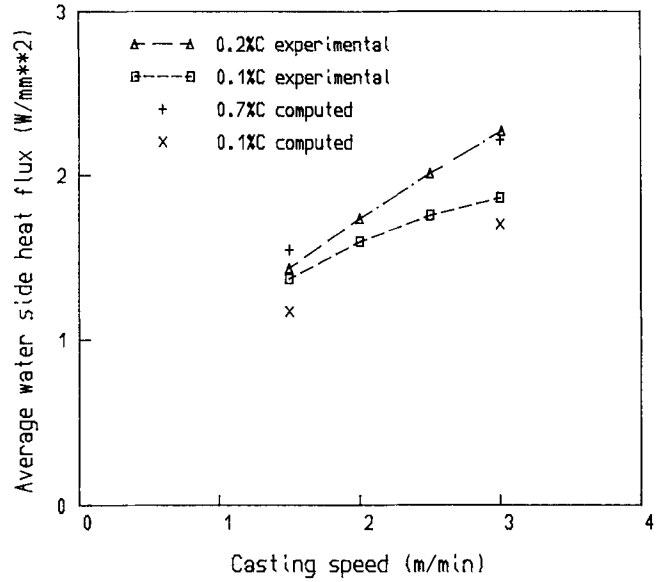

Fig. 10—The average water side heat flux from the Mannesmann mold *vs* casting speed.

and is hereafter referred to as the H142 mold. Casting was modeled for several grades (0.1 pct C, 0.4 pct C, and 0.7 pct C) in this mold, using a casting speed of 50.8 mm/s and considering mold tapers of both zero (untapered H142) and 0.6 pct/m (tapered H142). Results from these simulations are compared below to data presented in References 4 and 10.

The third mold, the Singh mold, was based on that used by Singh and Blazek,[3] having inside diameter of 93.6 mm, wall thickness of 5 mm, and length 425 mm. Singh and Blazek's mold was actually thicker than 5 mm, but the water passages were located at this distance from the hot face. Numerical experiments showed relatively little sensitivity of the displacement solution to mold thickness. Because the mold used in the experiments was untapered, this mold was considered only in untapered form. Simulations were performed using the same grades as above, but with a casting speed of 21.8 mm/s, corresponding to the speed used in the experiments. Selected results are compared below to data presented in Reference 3. The FEM mesh for all of the square mold cases had the same number of nodes and elements as used in the Mannesmann mold.

In Figure 11, computed temperatures at 3.2 mm from the cold face of the tapered H142 mold, casting 0.4 pct C steel, are shown in comparison to experimental measurements by Samarasekera *et al.*,[4] in a square mold. The corners of a square billet shrink a great deal more than the mid faces which remain close to the mold, leading to the differences in temperature found at these two locations. In contrast, the round billet shrinks uniformly, and thus one might expect the values computed for the round to lie between the off-corner and mid-face measurements. In fact, the computed values lie very close to the arithmetic mean of the measurements in those two locations, except at the meniscus, where the computed value is somewhat low.

Figures 12 and 13 show computed water-side heat fluxes in the Singh mold for 0.1 pct C and 0.4 pct C steels compared to corresponding data reported by Singh and Blazek.[3] Although the calculations show a decrease in heat flux for

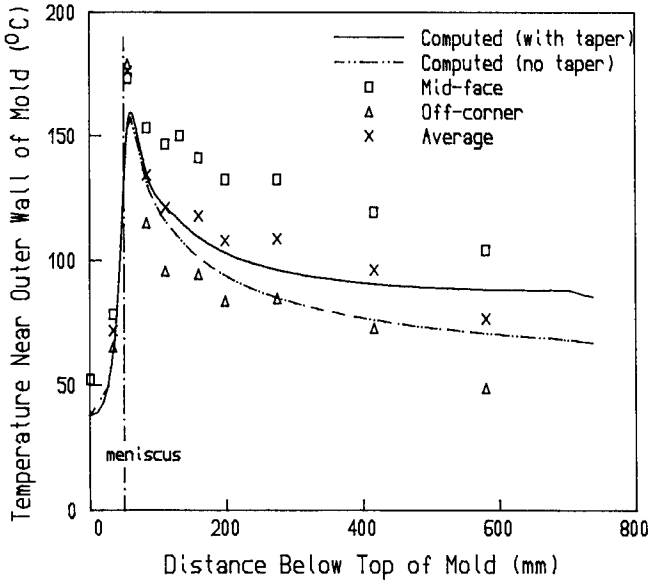

Fig. 11—Computed (0.4 pct C) temperature profiles 3.2 mm from the outer wall of the H142 mold, compared with experimentally measured values for 0.35 pct C at mid-face and off-corner locations.

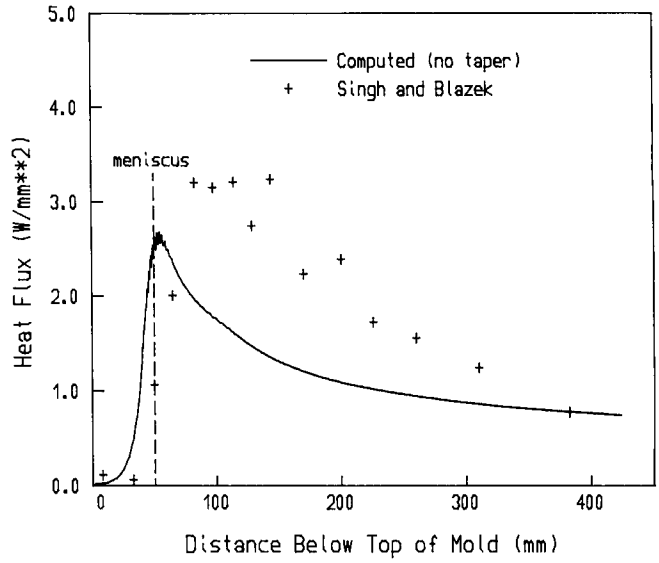

Fig. 13—Computed and experimentally measured[3] water side heat flux profiles for 0.4 pct carbon steel.

0.1 pct C steel compared to 0.4 pct C, the difference is less than was observed in the experiments. The peak flux is somewhat lower, and the peak is somewhat sharper in the calculations than in the experiments. Similar differences between rounds and squares have been observed by Nilsson *et al.*,[20] who reported much larger average heat fluxes and more peaked profiles, in comparison to those found in square billets. Thus, we attribute the discrepancies between the calculations and the experiments more to differences in geometry, rather than differences in phenomenology.

The lower heat flux found in 0.1 pct C steel compared to other grades has been associated with the poor surface quality and increased cracking tendency of this grade.[3,14,22,23] This phenomenon is usually explained as being due to the significant volume shrinkage accompanying the δ-γ phase transformation experienced by 0.1 pct C steel just after freezing. This enters the model through the linear thermal expansion coefficient, which is markedly different for 0.1 pct C compared to 0.4 pct C and 0.7 pct C (see Figure 14). Although 0.4 pct C steel also undergoes the δ-γ phase transformation, it does so at just 30 pct solid, and hence does not contribute to billet shrinkage in the model.

A. *Effect of Mold Taper*

As indicated in the study of industrial practices conducted by Brimacombe *et al.*,[10] it is common practice to taper billet molds to attempt to compensate for gap formation. The design of mold taper represents one of the instances where a reliable mathematical analysis would offer an attractive alternative to an expensive experimental program. Billet mold taper design has sometimes been done by examining

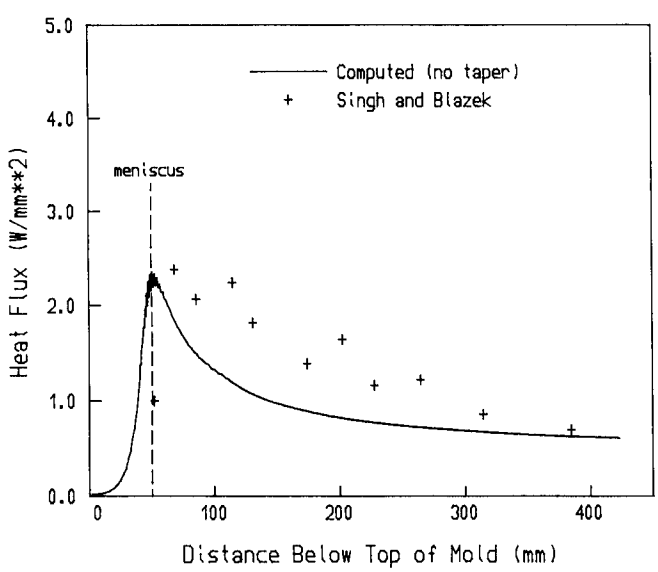

Fig. 12—Computed and experimentally measured[3] water side heat flux profiles for 0.1 pct carbon steel.

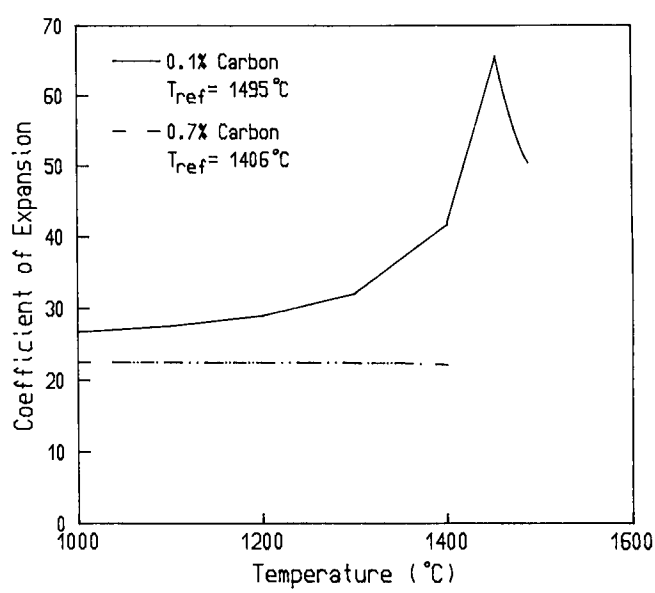

Fig. 14—Average coefficient of linear thermal expansion *vs* temperature for 0.1 pct and 0.7 pct carbon steel.

heat flux measurements on a mold with one taper, inferring the gap distribution, and adding or subtracting taper to specify a new mold.[23,24] Although the distorted mold is certain to be affected by the new taper, it is unlikely to be simply additive.

The effect of mold taper on computed air gap size in the H142 mold is shown in Figure 15. The main difference found between the mold with 0.6 pct/m taper and the untapered mold was that, beginning about 200 mm below the meniscus, the gaps become essentially constant for the tapered mold, while they continue to increase for the untapered mold. Figure 16 illustrates the net result of the changes in heatflux due to mold taper and the mold distortion along its length for two different grades. In both cases, the maximum displacement is unaffected by taper because the peak flux occurs close to the contact region. Taper mainly changes the shape of the profile below this region.

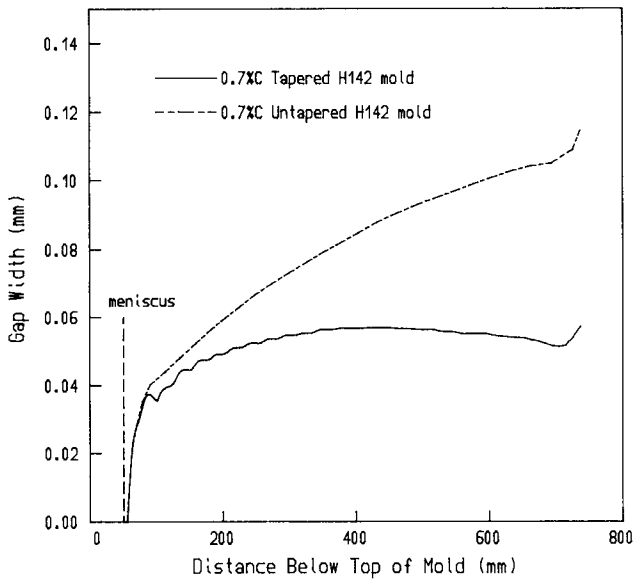

Fig. 15—Effect of taper on computed gap width profiles for 0.7 pct carbon steel cast in the H142 mold.

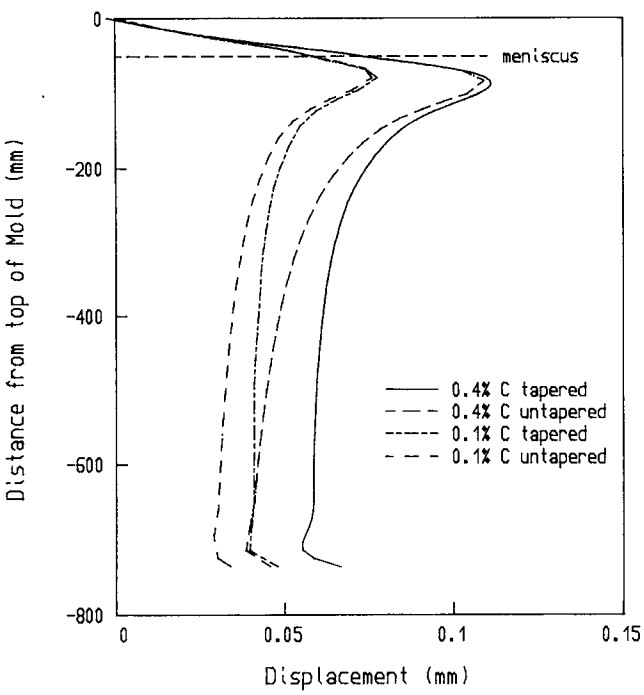

Fig. 16—Displacement of the hot face for the tapered and untapered H142 mold casting 0.1 pct C and 0.4 pct C steel.

The model indicates that the relationship between the gap size and mold taper is complex. Both mold distortion and shell shrinkage are significantly greater in the tapered mold. Hence, increases in mold taper produce less than proportional decreases in gap size and increases in heat flow. Because of this, it is not possible to obtain the gap profile for the tapered mold by simply subtracting the taper from the gap profile calculated using the untapered mold. This finding has important implications for mathematical analyses in which the air gap and temperature distribution are not coupled, and for cases where one wishes to extrapolate from one set of experimental results to other casting conditions.

B. *Stress and Fracture*

Another interesting result comes from examination of the computed stresses for 0.1 pct C and 0.7 pct C steels. In all cases, the largest tensile stress was the hoop stress, indicating that if cracks were to form they would be in the longitudinal direction. Figure 17 shows the computed hoop stresses and temperatures for both 0.1 pct C and 0.7 pct C cast in the Mannesmann mold. It can be seen that the tensile hoop stress in the crack-susceptible region is much larger for 0.1 pct C, indicating that this grade would be much more likely to crack than 0.7 pct C. These predictions agree quite well with experimental observations.[25,26] Figure 17 also shows how the sudden change in the surface heat transfer coefficient at the mold exit can severely increase the stresses in the strand. It shows that for both 0.1 pct C and 0.7 pct C cracks could form 6 to 9 mm below the surface of the strand because of the low heat transfer coefficient used at the mold exit in this model. Surprisingly, the model indicated that the tensile stresses for 0.1 pct C in the brittle region could be reduced by eliminating mold taper (see Figure 17). Unfortunately, the calculated shell thickness at the mold exit decreases to less than 5 mm, indicating the danger of breakout.

IV. DISCUSSION

A measure of the utility and accuracy of the proposed model for the continuous casting process is demonstrated by the number of important experimental observations and trends which have been reproduced in the calculations. Because the physical properties and process data are entered into the model, and the associated temperatures and stresses are computed without any adjustment to improve the fit with experimental observations, we believe that using this method can greatly increase the effectiveness of mathematical models to improve casting process design. However, we must caution that the model is highly dependent on the high temperature properties of the steels and gap medium, which are often not known to great precision.

The results obtained to date show excellent agreement with experimental results where the physics are represented most accurately, *i.e.*, in round billets. There are clear limits, however, to the direct application of these results to square cross-sections. Nilsson *et al.*[20] observed that the heat

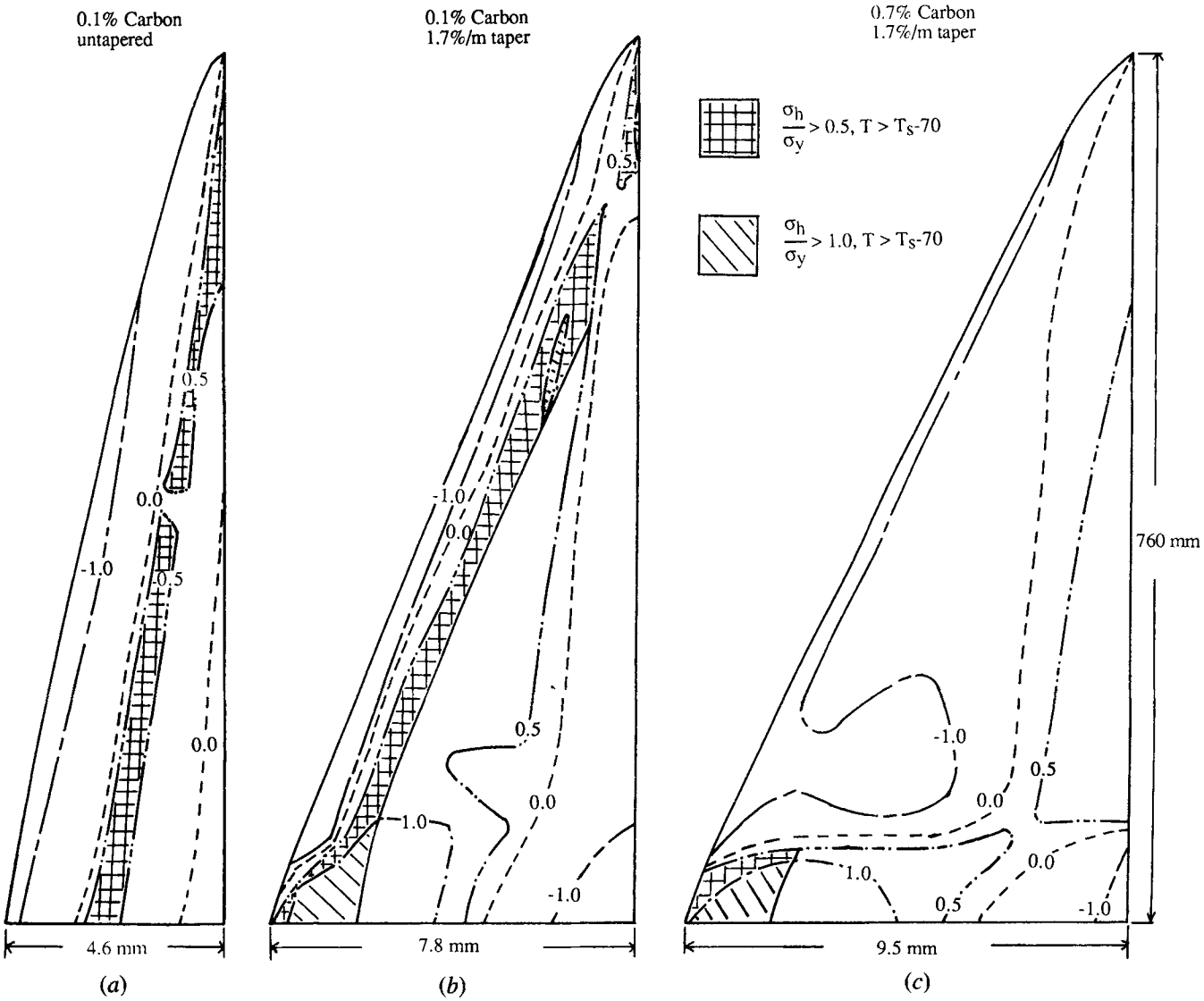

Fig. 17—Contours in the shell of hoop stress divided by the yield stress and regions (hatched) in the shell with potential for crack growth for 0.1 pct C in the untapered H142 mold and both 0.1 pct C and 0.7 pct C cast in the Mannesmann mold. Regions with potential for crack growth have both $\sigma_{hoop}/\sigma_{yield} > 1.0$ and $T > T_{solidus} - 70$ °C.

fluxes from round billets are consistently greater than those reported from squares of similar size. Our results indicate that this is partly due to the much larger tapers that they used and partly due to geometry differences. The computed and measured heat flux profiles on the rounds agree well with each other, but are much more sharply peaked than those found in square billets. We conclude from this that the air gap formation and stress development is quite different in square billets than in rounds. This is consistent with the observation of Brimacombe *et al.*[10] that the manner in which the mold is constrained plays a key role in the entire casting process. Testing of the ability of the model to predict three-dimensional aspects of the problem must await the extension of this work to three dimensions.

There remain a number of phenomena in continuous casting which cannot be evaluated with the present model. Oscillation marks and meniscus marks could not be predicted because they are associated with transient aspects of the process, not included in the model. The results in the example problem suggest that meniscus marks would form, because the computed liquidus does extend onto the meniscus (see Figure 7). This would lead to periodic freezing and runover, which produce surface depressions by the mechanism suggested by Tomono *et al.*[27] Similarly, periodic mold oscillation also produces surface depressions, as described by Samarasekera *et al.*[4] In the latter paper, the surface defects were shown to play an important role in the local heat transfer, and thus would have to be modeled in a more complete analysis of the casting process.

In a similar vein, there are a host of important phenomena found in billet casting which originate in the three-dimensional aspects of production casters. Among these are the effects associated with the corners in square molds, where many problems relating to internal cracking and surface defects begin. Also, most casters now used curved molds to eliminate the requirement for bending the strand, which results in different thermal behavior at the curved faces than at the flat faces.

The present model for fluid flow is quite crude, and must be improved to examine the details of the flow patterns in the liquid associated with the incoming stream. In particular, an improved model could address phenomena such as shell erosion, white-band formation due to fluid flow, and electromagnetic stirring. The work of Figueira and Szekely[28] and Spitzer *et al.*[29] provides confidence that the techniques exist to include this aspect of the process. Extension of the model to examine these effects would certainly bring about a much heavier computational load. However, the results achieved to date suggest that the exercise would be fruitful.

V. CONCLUSIONS

A mathematical model has been developed to analyze heat transfer and stress development in the mold region of round continuous casters. The model uses both thermal and stress analysis to derive a self-consistent solution for the temperature distributions in the strand and mold, along with the size of the gap between the shell and mold formed by thermal distortion. The model predictions have been found to agree very well with available experimental data for round casters. Specifically:

1. The heat flux curve for round casters has a high peak in the vicinity of the meniscus which subsequently drops abruptly due to rapid formation of an air gap. In molds with high taper, the curve then rises toward the mold exit, while with low taper, it decreases slowly toward the mold exit.
2. The physical properties of 0.1 pct C steel, particularly the volume shrinkage associated with the delta-ferrite to austenite phase transformation, are responsible for the reduced heat fluxes found when casting this grade.
3. At the same time, the resultant stress state accounts for the greater propensity for 0.1 pct C to develop longitudinal cracks, in comparison to other grades.
4. Higher tapers produce higher heat fluxes, but the correspondence is not directly proportional.
5. Round billets and square billets behave very differently in several important respects that may have important implications on quality.

The results of this work have shown that the interaction between mold taper, mold distortion, and air gap formation has an important effect on heat transfer in a continuous billet casting machine, and can be examined in a comprehensive mathematical analysis. Many important phenomena remain to be added to the model. These include transient behavior relating to oscillation and meniscus mark formation, three-dimensional effects such as the corners of square molds and opposing faces in curved molds, and improved modeling of fluid flow.

APPENDIX A

Thermal conductivity of gas in the shell-mold gap

In this discussion, the gap medium is assumed to contain a mixture of 80 pct air and 20 pct hydrogen. Akimenko and Skvortsov[30] have suggested that this composition would result from the use of rapeseed oil as a lubricant. According to Burmiester,[31] the thermal conductivity of a binary mixture of gases can be calculated from the conductivity of its components as follows:

$$K_m = \beta K_L + (1 - \beta) K_R \qquad [A.1]$$

where K_m is the conductivity of the mixture, and β is an empirical constant that varies from 0.3 to 0.8, chosen in this analysis to be 0.5. K_L is a linear combination of the component conductivities:

$$K_L = X_1 K_1 + X_2 K_2, \qquad [A.2]$$

where X_i is mass fraction of each component in the mixture and K_i is the thermal conductivity of each component. K_R is a reciprocal combination of the component conductivities:

$$\frac{1}{K_R} = \frac{X_1}{K_1} + \frac{X_2}{K_2} \qquad [A.3]$$

with X_i and K_i defined as above.

Burmiester[31] also suggested a relationship between the conductivity of a gas and its absolute temperature:

$$K = A\sqrt{T}\,\frac{1 + GT}{1 + S/T} \qquad [A.4]$$

where A, G, and S depend on the gas.

This relationship gave a good fit to the data presented in Ozisik[32] for both air and hydrogen. An iterative best fit scheme was used to find the values of A, G, and S, resulting in the following relationships:

$$K_{\text{air}} = \sqrt{T}\,\frac{(1.90 \times 10^{-7}T + 1.34 \times 10^{-3})}{(1 - 11.2/T)} \qquad [A.5]$$

$$K_{H_2} = \sqrt{T}\,\frac{(6.11 \times 10^{-7}T + 1.02 \times 10^{-2})}{(1 + 23.2/T)} \qquad [A.6]$$

Table I shows the resulting temperature dependence of a 20 pct hydrogen-air mixture.

APPENDIX B

Physical properties of plain carbon steel and copper mold material

The following tables (II through VIII) give the properties used in the simulations. Intermediate values were determined using piecewise linear interpolation.[8]

The average coefficients of linear thermal expansion were calculated using the formula:

$$\bar{\alpha}_{\text{thermal}} = \frac{\left(\frac{V}{V_{\text{ref}}}\right)^{1/3} - 1}{T - T_{\text{ref}}} \qquad [B.1]$$

Table I. Conductivity of a 20 Pct Hydrogen-Air Mixture

Temperature (°C)	Conductivity (W/mK)
200	0.054
400	0.065
600	0.076
800	0.086
1000	0.096
1200	0.105
1400	0.114

The specific volume V was calculated using the following equations derived from Wray:[14]

$$V_{\delta\text{-iron}} = [8.154(C) + 0.1234 + 9.38 \times 10^{-6}(T - 20)] \times 10^{-3}\ \mathrm{m^3/kg} \quad [B.2]$$

$$V_{\gamma\text{-iron}} = [7.688(C) + 0.1225 + 9.45 \times 10^{-6}(T - 20)] \times 10^{-3}\ \mathrm{m^3/kg} \quad [B.3]$$

where T is temperature in °C and C is weight percent carbon in the alloy.

In the δ-γ region, the following was used:

$$V(T) = f_\gamma V_\gamma + (1 - f_\gamma)V_\delta \quad [B.4]$$

where f_γ is the fraction of austenite present, determined using the lever rule on the equilibrium phase diagram.

APPENDIX C

Mold-water heat transfer coefficient

The mold-water heat transfer coefficients used in the simulations are listed in Table IX. These data were calculated using the procedure described by Rohsenow *et al.*[36] In this procedure they suggest the use of an equation for fully developed forced convection nucleate boiling due to Thom *et al.*:[37]

$$T_W - T_S = 0.0225e^{-0.00115p}[q_b]^{0.5} \quad [C.1]$$

where T_W is the wall temperature in °C; T_S is the water saturation temperature in °C, p is the water pressure in kPa; and q_b is the boiling heat flux in W/m^2. A recent evaluation of correlations such as Eq. [C.1] by Guglielmini[38] showed that the following correlation by Stephan and Auracher[39] gave a better fit to experimental data for the low pressure ranges one normally finds in continuous casting molds:

$$T_W - T_S = \frac{1}{C} q_b^{0.327} \quad [C.2]$$

Table IV. Strength of 0.1 Pct Carbon Steel at a Strain Rate of $4 \times 10^{-4}\ s^{-1}$[12]

Temp. (°C)	Elastic Modulus GPa	Yield Stress MPa	Plastic Modulus MPa
900	20.46	20.46	1224.0
1200	7.738	7.738	555.6
1400	4.3	4.3	330.7
1455	3.385	3.385	278.8
1495	0.297	0.297	25.0
1520	0.026	0.026	2.24
1600	0.026	0.026	2.24

Table V. Strength of 0.4 Pct Carbon Steel at a Strain Rate of $4 \times 10^{-4}\ s^{-1}$[12]

Temp. (°C)	Elastic Modulus GPa	Yield Stress MPa	Plastic Modulus MPa
900	17.2	17.2	1600.0
1200	6.1	6.1	350.0
1416	2.88	2.88	100.0
1456	0.251	0.251	7.75
1496	0.022	0.022	0.6
1600	0.022	0.022	0.6

Table II. Effective Specific Heat of Plain Carbon Steel[33]

Temperature (°C)	0.1 Pct Carbon (kJ/kgK)	Temperature (°C)	0.4 Pct Carbon (kJ/kgK)	Temperature (°C)	0.7 Pct Carbon (kJ/kgK)
0	0.62	900	0.616	0	0.77
900	0.62	1456	0.7	700	0.77
1450	0.7	1473	8.89	750	2.08
1453.4	1.2	1489	8.91	800	0.61
1495	0.94	1506	0.75	1406	0.69
1500	10.66	1600	0.75	1416	4.58
1520	10.66			1476	4.58
1530	0.75			1486	0.69
1600	0.75			1530	0.7
				1600	0.75

Latent heat of fusion of iron = 273 kJ/kg[33]

Table III. Thermal Conductivity of Plain Carbon Steel Data[33]

Temperature (°C)	0.1 Pct Carbon (W/mmK)	Temperature (°C)	0.4 Pct Carbon (W/mmK)	Temperature (°C)	0.7 Pct Carbon (W/mmK)
0	0.03	0	0.03	0	0.03
700	0.03	700	0.03	700	0.03
1100	0.025	1100	0.025	1100	0.025
1495	0.033	1456	0.033	1406	0.033
1530	0.027	1506	0.027	1486	0.027
1540	0.05	1540	0.05	1540	0.05
1600	0.05	1600	0.05	1600	0.05

The conductivity of the liquid steel has been increased by a factor of 2 to simulate turbulent convection.

Table VI. Strength of 0.7 Pct Carbon Steel at a Strain Rate of 4×10^{-4} s^{-1}[12]

Temp. (°C)	Elastic Modulus GPa	Yield Stress MPa	Plastic Modulus MPa
900	17.763	17.763	1002.0
1150	7.132	7.132	460.0
1366	3.242	3.242	162.8
1406	0.28	0.28	13.9
1446	0.024	0.024	1.2
1546	0.024	0.024	1.2

Table VII. Coefficient of Linear Thermal Expansion of Copper[34]

Temperature (°C)	Coefficient of Expansion at T_{ref} = 20 °C $(K)^{-1}$
15	15.2×10^{-6}
71	15.7×10^{-6}
127	16.5×10^{-6}
227	17.6×10^{-6}
327	18.3×10^{-6}

Table VIII. Other Physical Properties of Copper Mold[35]

Thermal conductivity	0.38 W/mmK
Elastic modulus	1.1×10^5 N/mm
Poisson's ratio	0.36

Table IX. Mold-Water Heat Transfer Coefficient (Water Velocity 8 m/s)

Mold Wall Temperature (°C)	Heat Transfer Coefficient (W/mm^2 K)
0	0.03
120	0.03
125	0.031
130	0.034
135	0.041
140	0.054
145	0.07
150	0.09

where C is a pressure dependent parameter. For a pressure of 100 kPa, $C = 3.7$. The heat transfer coefficient calculated from correlations such as [C.1] and [C.2] can differ by as much as 100 pct,[38] so the effects of both correlations on the solution were compared. However, both resulted in nearly identical fluxes, and a maximum difference in peak water side temperature of 4 °C. This is because the air gap is the dominant resistance to heat flow.

ACKNOWLEDGMENTS

This work has been sponsored by the National Science Foundation, under grant DMC-85-11378, for which the authors are grateful. They also wish to thank Peter Wray, Ken Blazek, and Ishmael Saucedo of Inland Steel Corporation, and Keith Brimacombe of the University of British Columbia for helpful discussions and suggestions through the course of this work.

REFERENCES

1. A. W. D. Hills: *J. Iron Steel Inst.*, 1965, vol. 203, pp. 18-26.
2. A. Perkins and W. R. Irving: *Math. Process Models in Iron and Steel Making*, Metal Society, London, 1975, pp. 187-99.
3. S. N. Singh and K. E. Blazek: *J. Metals*, 1974, vol. 10, pp. 17-27.
4. I. V. Samarasekera, J. K. Brimacombe, and R. Bommaraju: *ISS Trans.*, 1984, vol. 5, pp. 79-94.
5. A. Grill, K. Sorimachi, and J. K. Brimacombe: *Metall. Trans. A*, 1976, vol. 7A, pp. 177-89.
6. J. O. Kristiansson: *J. of Thermal Stresses*, 1984, vol. 7, pp. 209-26.
7. M. S. Engelman: *FIDAP Theoretical Manual-Revision 3.10*, Fluid Dynamics International, Inc., Evanston, IL, 1986.
8. J. O. Hallquist: NIKE2D UCID-19677, Lawrence Livermore National Laboratory, Livermore, CA, 1983.
9. E. A. Mizikar: *Trans. AIME Metallurgical Society*, 1967, vol. 239, pp. 1747-53.
10. J. K. Brimacombe, E. B. Hawbolt, and F. Weinberg: *ISS Trans.*, 1982, vol. 1, pp. 29-40.
11. M. A. Perzyk: *Materials Science and Technology*, 1985, vol. 1, pp. 84-92.
12. P. J. Wray: *Metall. Trans. A*, 1982, vol. 13A, pp. 125-34.
13. J. K. Brimacombe and K. Sorimachi: *Metall. Trans. B*, 1977, vol. 8B, pp. 489-505.
14. P. J. Wray: in *Modeling of Casting and Welding Processes*, H. D. Apelian and H. D. Brody, eds., Met. Soc. AIME Conf., 1980, pp. 245-57.
15. H. C. Suzuki, S. Nishimura, and Y. Nakamura: *Proc., 100th ISIJ Meeting*, Oct. 1980, #S805.
16. K. Sorimachi and J. K. Brimacombe: *Ironmaking and Steelmaking*, 1977, vol. 4, pp. 240-45.
17. J. E. Lait and J. K. Brimacombe: *ISS Trans.*, 1982, vol. 1, pp. 1-13.
18. J. Dubendorff, J. Sardemann, and K. Wunnenberg: *Stahl u. Eisen*, 1983, vol. 103, no. 25/26, pp. 1327-32.
19. K. Wunnenberg and H. Jacobi: *Stahl u. Eisen*, 1984, vol. 104, no. 23, pp. 1213-18.
20. H. Nilsson, H. Schrewe, and H. Jacobi: *Stahl u. Eisen*, 1987, vol. 107, no. 5, pp. 217-24.
21. L. Saroff: in *Continuous Casting, Proc., Continuous Casting Symp. of the 102th AIME Annual Meeting*, K. R. Olen, ed., Warrendale, PA, 1973, pp. 323-40.
22. P. W. Baker and J. F. Grandfield: in *Solidification Processing 1987*, H. Jones, ed., Sheffield, U.K., 1987, pp. 227-29.
23. I. G. Davies, K. Thomas, J. Gorringe, and K. A. Broome: in *Continuous Casting '85*, Book 326, The Institute of Metals, London, 1985, pp. 25.1-25.10.
24. R. J. Dippenaar, I. V. Samarasekera, and J. K. Brimacombe: *ISS Transactions*, 1986, vol. 7, pp. 31-43.
25. H. F. Schrewe, J. Ehrenberg, J. Sardemann, and H. E. Nilsson: in *Continuous Casting '85*, Book 326, The Institute of Metals, London, 1985, pp. 22.1-22.8.
26. A. Etienne and W. R. Irving: in *Continuous Casting '85*, Book 326, The Institute of Metals, London, 1985, pp. 1.1-1.9.
27. H. Tomono, W. Kurz, and W. Heinemann: *Metall. Trans. B*, 1981, vol. 12B, pp. 409-11.
28. R. M. Figueira and J. Szekely: *Metall. Trans. B*, 1985, vol. 6B, pp. 67-75.
29. K. Spitzer, M. Dubke, and K. Schwerdtfeger: *Metall. Trans. B*, 1986, vol. 17B, pp. 119-31.
30. A. D. Akimenko and R. A. Skvortsov: *IZV. VUZ Chernaya Metall.*, 1958, vol. 12, pp. 45-50.
31. L. L. Burmiester: *Convective Heat Transfer*, Wiley, New York, NY, 1983, pp. 57-69.
32. M. N. Ozisik: *Basic Heat Transfer*, McGraw-Hill, New York, NY, pp. 498-500.
33. R. D. Pehlke *et al.*: *Summary of Thermal Properties for Casting Alloys and Mold Materials*, University of Michigan, NTIS-PB83-211003, 1982.
34. R. Touloukian, R. W. Powell, C. Y. Ho, P. G. Clemens, E. H. Buyco, and D. P. DeWitt: *Thermophysical Properties of Matter*, Purdue Research Foundation, West Lafayette, IN, vols. 1, 4, 7, and 12, 1975.
35. Z. D. Jastrzebski: *The Nature and Properties of Engineering Materials*, John Wiley and Sons, New York, NY, 1977.
36. W. M. Rohsenow, J. P. Hartnett, and E. N. Ganic: *Handbook of Heat Transfer*, 2nd ed., McGraw-Hill, New York, NY, 1985, pp. 12-41, 12-44.

37. J. R. S. Thom, W. M. Walker, T. A. Fallon, and G. E. S. Reising: *Proc., Inst. Mech. Engr.*, 1966, 3C, vol. 180, pp. 226-46.
38. G. Guglielmini, E. Nannei, and C. Pisoni: *Warme und Stoffubertragung*, 1980, vol. 13, pp. 177-85.
39. K. Stephan and M. Auracher: *Int. J. Heat and Mass Transfer*, 1981, vol. 24, pp. 99-107.